RSC Advances

Photoluminescence enhancement from silicon quantum dots located in the vicinity of a monolayer of gold nanoparticles

A.L. Muñoz-Rosas[a], A. Rodríguez-Gómez[b], J.A. Arenas-Alatorre[b], J.C. Alonso-Huitrón[a]*

[a]Instituto de Investigaciones en Materiales, Universidad Nacional Autónoma de México, A.P.70-360, Coyoacán04510, México D. F., México

[b]Instituto de Física, Universidad Nacional Autónoma de México, A.P.20-364, Coyoacán01000, México D. F., México

1

Graphical Abstract
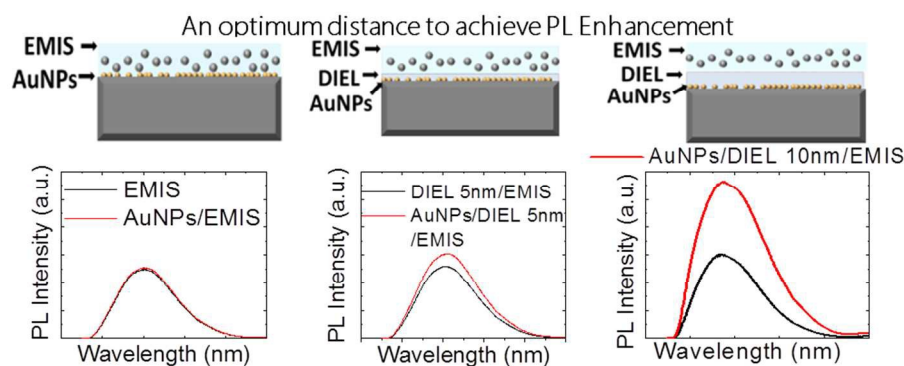
Abstract

In this paper we show that it is possible to carry out a functional coupling between a thin film of silicon quantum dots embedded in a silicon nitride matrix (SiQDs) and a monolayer of gold nanoparticles by using dry and low temperature techniques, such as those used in microelectronics industry, i.e., Remote Plasma Enhanced Chemical Vapor Deposition (RPECVD) and Sputtering. The coupled structure showed 105% of photoluminescence (PL) enhancement, compared with PL observed from the SiQDs without the gold monolayer. The SiQDs used as light emitters have an average diameter of 3.1 nm, a particle density of $6.04E^{12}$ particles/cm^2 and a maximum PL peak at 505 ±5nm. Additionally, the gold nanoparticles were designed with the following characteristics: the particles are embedded in a silicon nitride matrix, show quasi-spherical shapes, an average diameter of 2.9nm, a particle density

of $2.52E^{12}$ particles/cm^2 and their surface plasmon resonance is located at 540 ±3nm. We found that there is an optimum separation distance between SiQDs and the gold monolayer to achieve the maximum photoluminescence enhancement. For our structure, such optimal distance was 10±1nm. We consider that there could be two combined physical effects responsible of the enhancement: a) a plasmonic diffraction-limited coupling and b) a change of the scattering mechanisms of the primary laser light.

Introduction

Silicon is extensively used in photovoltaic and microelectronics industries due to its physical characteristics, abundance and its relative ease manipulation[1–3]. However, silicon photonic applications are scarce because as an indirect band semiconductor its emission efficiency is very low[4].

Several works have reported that when silicon is confined in spherical three-dimensional regions of not more than 10 nm in diameter, a slight alignment between the maximum of the valence band and the minimum of the conduction band occurs. This phenomenon is known as quantum confinement effect (QCE)[5–12]. The QCE greatly improves the silicon photoluminescent (PL) and electroluminescent (EL) efficiencies to rates of about 2%, but additionally, QCE allows the modulation of the emission energy[13–19].

By using the QCE some research groups have tried to manipulate silicon at the nanoscale to fabricate multiple luminescent devices ranging from ambient lighting to light emitting diodes (LEDs) for multiple purposes[20–22]. Unfortunately, although the EL emission efficiencies have improved due to the QCE[23,24], these are not yet enough to contrive the full range of silicon-based devices that the modern society demands.

Some research works have observed a considerable improvement of the integrated emission intensity from silicon emitting quantum dots (SiQDs) when these are adequately coupled with nanostructured noble metal particles[25–35]. Therefore, the fabrication of coupled silicon-metal nanostructures could be one possible solution for the manufacture of multiple luminescent devices based on silicon[36]. However, it must be emphasized that fabrication processes to make silicon-noblemetal coupling structures which show photoluminescence enhancement are not simple. Indeed, to our knowledge, the best enhancements ratios from these kind of structures have been reported by two research groups (Biteen et al. and Benami et al.) [26–31], and both groups are characterized by using similar equipment and methodologies for their preparation.

In those works published by Biteen et al. the used methodology can be summarized in four steps: i) implantation of Si^+ ions into a SiO_2 substrate, ii) three-stage annealing into argon or hydrogen atmospheres to generate SiQDs and to eliminate defect states in SiO_2 matrix, iii) substrate etching by using an aqueous HF solution to diminish the distance from the substrate surface to the implanted SiQDs, and iv) deposition of a nanoporous gold layer over the etched surface of SiO_2, or else, fabrication of a silver particles pattern by means of nanolithography. Meanwhile, Benami et al. carry out steps i) and ii) in akin way to Biteen's methodology, and add a third step in which the sample is implanted with Ag^{+2} ions at different energies to vary the distance between the SiQDs and the silver nanoparticles that are formed after a second annealing process.

The results provided by both groups are encouraging, because they throw light on two alluring effects observed when nanoconfined silicon particles are located in the vicinity of noble metals nanoparticles. First, they provide experimental evidence of twofold to even threefold PL enhancement, compared to the PL from those SiQDs which are not coupled. Second, they report

different degrees of PL quenching when SiQDs are placed right next to metal particles in an homogenous mixture. To wit, those effects allow us to glimpse that distances between silicon and metal particles are critical in order to prevent quenching and to achieve enhancements. However, there are three unattended issues we believe must be addressed in order to harness this PL enhancement effect in designing functional commercial devices, which are: a) fabrication techniques must be highly compatible with those used in microelectronic industry, b) it is essential to give a comprehensive description of particle characteristics of both metal and SiQDs, and c) it should be clarified the existent relationship between PL enhancement and the separation distance between SiQDs and metal particles.

In this work, we have tailored a multilayered structure (coupling silicon to gold) which exhibits a twofold PL enhancement. For its fabrication, we have combined Remote Plasma Enhanced Chemical Vapor Deposition (RPECVD) and Sputtering techniques into a method which has a very strong rapport with those used in the microelectronics industry, i.e. dry, low temperature, economical and fast depositions. Further, our paper offers a thorough study of size and particle density of both gold and silicon nanoparticles; and it is also briefly discussed the role played by the surrounding medium in which particles are embedded when the PL enhancement is achieved. Finally, our methodology allowed us to carry out a good analysis of the separation distances between SiQDs and the monolayer of gold nanoparticles (AuNPs) in order to obtain PL enhancement.

Experimental Section

The AuNPs were deposited using a Cressington 108 Sputter Coater with Au target (99.9999% purity) in 0.8 mbar Argon atmosphere. Quartz and silicon n-type (100) high resistivity (200

Ωcm) were used as substrates. Prior to deposition, quartz substrates were solvent cleaned with trichloroethylene and acetone. Silicon substrates were dipped in P-etch solution to remove native oxide[37]. Two thin films of silicon nitride with different chemical compositions and thickness were deposited using a Remote Plasma Enhanced Chemical Vapor Deposition (RPECVD) system whose characteristics have been reported previously[38]. Substrate temperature of 300°C, radio frequency power of 150 W and pressure of the reaction chamber of 300mT were used as deposition parameters. The flow rates of H_2, Ar and SiH_2Cl_2 were 10, 75 and 5 sccm respectively for all the deposited films. Flow rate of NH_3 was settled in 600 sccm for purposes of growing a non-radiative silicon nitride thin insulating film (DIEL) and 200 sccm for growing silicon quantum dots embedded in a chlorinated silicon nitride matrix film (EMIS). The thickness of these layers was varied for all the fabricated structures by controlling the deposition time.

Null ellipsometry was used to measure thickness (Th) of the films using a manual Gaertner 117 ellipsometer equipped with a He-Ne laser (λ=632 nm). Photoluminescence (PL) measurements were carried out in a totally dark room at ambient temperature using an unfocused beam of 25 mW from a Kimmon He–Cd laser operating at 325 nm (3.81 eV). The PL spectra were recorded with a Fluoromax-Spex spectrofluorometer using as signal detector an optical fiber normal to the sample emission. Ultraviolet–visible (UV–vis) transmission measurements were carried out in the range from 200 to 1100 nm using a double-beam PerkinElmer Lambda 35 UV–vis spectrophotometer. The shape, size and distribution of the AuNPs and SiQDs were confirmed by high resolution electron microscopy (HRTEM) and high angle annular dark field (HAADF) using a field emission gun (JEM-2010F) which operates at 200 kV near the Scherrer focus, with a theoretical point to point resolution of 0.19 nm. The HRTEM images in planar view of the samples were recorded with a CCD camera and treated with a digital analysis program. A

Field Emission-Scanning Electron Microscope (JEOL7600F FE-SEM) was used to observe shape and distribution of the AuNPs for different growing times.

Results and discussion

Taking into consideration the possible existence of an optimal separation distance between SiQDs and AuNPS for our system, we tailored our structure in three stages. First stage reports and discuss the methodology we used to fabricate the "emitter field", i.e., the deposition of the SiQDs by means of RPECVD. In this stage we also perform an analysis of our selected films (DIEL and EMIS) to be implemented in the final multilayered structure. In second stage we used Sputtering technique to fabricate the gold nanoparticles monolayer (AuNPs). Additionally, in second stage we discuss about the particle characteristics of the AuNPs, e.g. particle size, particle shape and particle density. Finally, in the third stage we performed the tuning between the SiQDs and AuNPs films, we did this engineering by varying the separation distances between the films and recording the PL changes from each coupled structure.

Fabrication and selection of the emission field (SiQDs)

Quantum confinement (QC) in silicon clusters can be identified as strong, medium and weak. Strong QC exists when the Bohr radius of the exciton is larger than the size of the confined system (~5.3 nm). The latter implies that the probability of radiative transitions from silicon nanoparticles will increase when particle diameters fall below 10 nm approximately, because their band energy will become quasi-direct[39]. Then, we might expect the maximum possible PL efficiencies for those emitter fields conformed by clusters with sizes below 5 nm. Therefore, our first design objective is to fabricate a set of thin films containing SiQDs with strong QC effect.

On the other hand, and in order to avoid in a feasible extent the non radiative recombination from charge carriers in our films, passivation of silicon quantum dots was carried out by means of a chlorinated precursor (SiH_2Cl_2) whose use has demonstrated diminished dangling bonds and therefore the non radiative localized states[40].

The Figure 1 contains the photoluminescence spectra of seven thin films constituted by SiQDs embedded in a silicon nitride matrix. Those samples were used in a previous study[41] and were deposited by using our RPECVD system with different NH_3 flow rates. With the exception of sample E, which has a film thickness of 375 nm, all other samples of the group have thicknesses ranging between 78 and 85 nm. The PL integrated intensity associated to each sample depends mostly on the amount of SiQDs the sample has, i.e., SiQDs density (Si-ρ); while the location of the maximum PL peak (MPLp) depends on the SiQDs average size (Si-Ø).
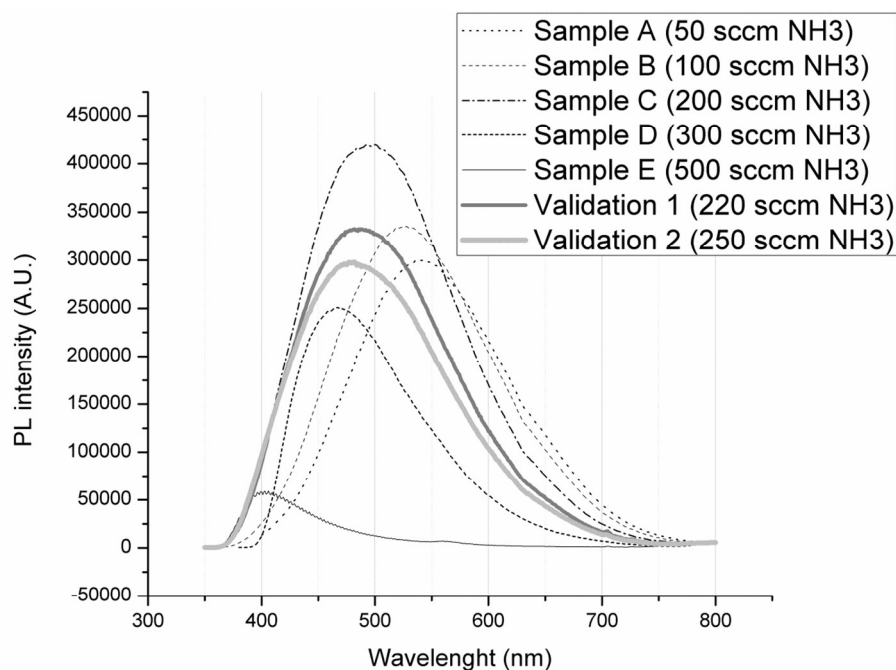
Figure 1. Photoluminescent spectra of seven thin films containing SiQDs embedded in a chlorinated silicon nitride matrix using different NH_3 flow rates. PL integrated intensity and location of the main peak are related to superficial density and average size of the particles respectively. "Reprinted from Materials Letters, 125 (2014) 44–47, A.Rodríguez, J.Arenas, A.L.Pérez-Martínez, J.C.Alonso, Role of ammonia in depositing silicon nanoparticles by remote plasma enhanced chemical vapor deposition, with permission from Elsevier"

By maintaining unaltered the previously reported deposition conditions[41], but feeding our RPECVD system with different ammonia flows (Aflow), we can change Si-Ø and therefore predict the MPLp of the deposited film. The linear model expressed in equation 1, is a tool that allows us to grow SiQDs in a controlled way[41].

$MPLp$= -0.3079*$Aflow$+557.6328 (1)

The model has an accuracy of 99% to fabricate SiQDs films with a maximum PL peak between 400 and 540 nm. However, it is important to take into consideration that blue shifts will sacrifice Si-ρ, with the consequent integrated intensity decrement. An appropriate example is seen in the emission spectrum of sample E from figure 1, which has a four times bigger thickness that sample C, but a ten times lower integrated intensity. Hence, when the Aflow rises up to 600 sccm it is possible to grow a film with Si-ρ very close to zero. A film with Si-ρ ≈ 0 could be considered as a pure silicon nitride dielectric ≈ Si_3N_4[42].

The Figure 2 shows the emission spectra from EMIS film (200 sccm Aflow) and DIEL film (600 sccm Aflow). DIEL and EMIS films have similar thicknesses, 96.5 and 97.9 nm respectively. However, EMIS has PL intensity 22 times higher than DIEL due to its higher Si-ρ. Additionally, DIEL film exhibits almost identical optical characteristics to those shown by stoichiometric silicon nitride reported elsewhere[42,43]. Therefore, in our structure design we will use DIEL type growths for all those design steps where a dielectric of Si_3N_4 is needed. One

HRTEM image of our DIEL film is available as supporting information (Supporting Figure 1).

Regarding the film thickness, it is worth to note that thickness in both EMIS and DIEL films can

be controlled by variations in the deposition times.
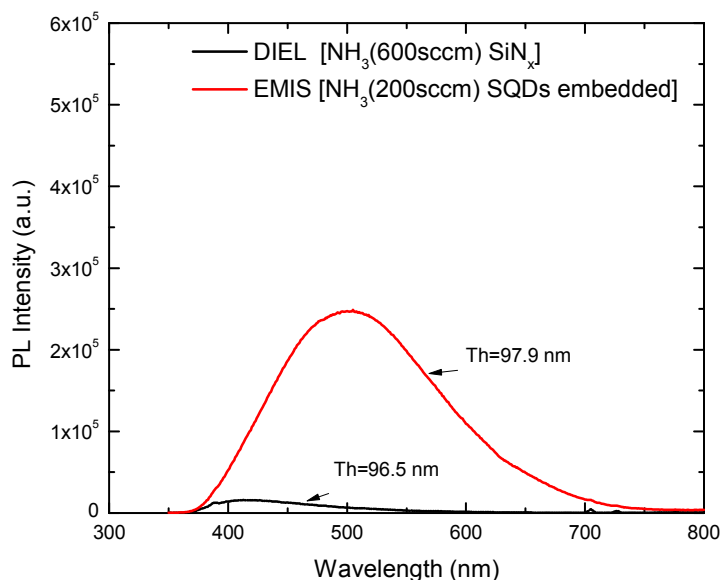
Figure 2. Comparison between emission spectra from EMIS (200 sccm Aflow) and DIEL (600 sccm Aflow). Both

films **have** about the same thickness. The integrated PL intensity from the EMIS layer is 22 times bigger than DIEL

layer.

A HAADF micrograph obtained from an EMIS film is shown in Figure 3. A uniform particle

distribution throughout the sample is observed, confirming a good Si-ρ/Si-Ø ratio. This ratio

gives rise to the largest PL integrated intensity within the range of 400-540 nm. A HRTEM

micrograph is shown in the inset a). The observed uniformity of the matrix indicates a very high

quality of stoichiometric silicon nitride. On the other hand, the low contrast between matrix and

SiQDs is expected due silicon is the base element in both components of the system. From inset

a) is also possible to see in detail the SiQDs morphology, most of the nanoparticles show

10

spherical shapes, but there are also some particles with prolate spherical shapes in a lower proportion. The identified spheroids shapes confirm a confinement in three directions and therefore their nature of emitting quantum dots.

Moreover, inset b) of Figure 3 shows a histogram with the SiQDs size distribution of EMIS film. The Si-Ø is 3.1 nm, while Si-ρ is about $6.04E^{12}$ particles/cm^2. By using well known equation 2 and a value of 1.16 eV to E_{SiBulk}, we calculated the quantum confinement constant C, resulting in a value of 11.9 nm^{2}eV, which is in good agreement with those confinement constants associated to other based silicon emitter fields reported elsewhere[6,7,44].

$$E_{PL} = E_{SiBulk} + C/d^2 \quad (2)$$
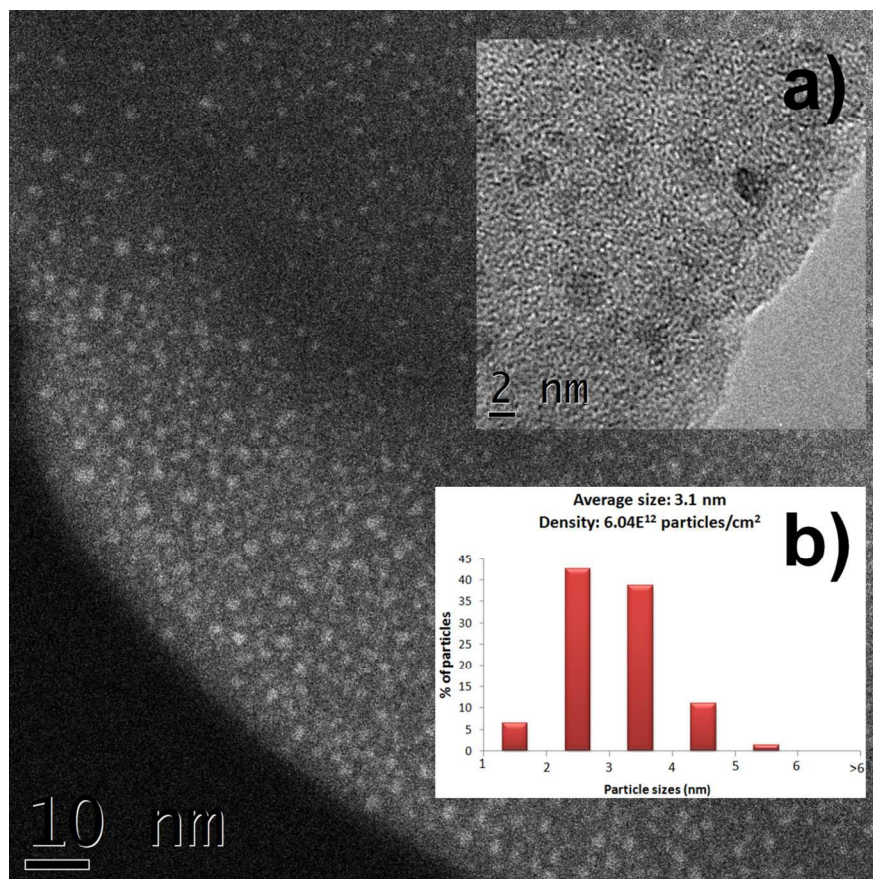
Figure 3. HAADF image obtained from an EMIS film. Uniform particle distribution throughout the sample is observed. Inset a) of this sample shows spherical shape of the SiQDs and therefore confinement in three dimensions

of the particles. Inset b) shows the histogram of the size distribution of the SiQDs. Average size is 3.1 nm and superficial density is about $6.04E^{12}$ particles/cm^2.

Thence, to use EMIS type depositions as the emitter field in our structure, vests the design with two advantages: a) EMIS film has the highest possible Si-ρ for a film grown in our RPECVD system, and consequently, the biggest PL integrated intensity. b) Since the emitter field is embedded in silicon nitride, no interface is going to be formed when DIEL layers are deposited under or over an EMIS film. The latter, avoids Fabry-Perot reflections, to the extent feasible [45,46].

Design of the gold monolayer (AuNPs)

Nanostructured noble metals show extinction plasmonic resonances in the visible section of the electromagnetic spectrum. Due that the location of these resonances depends on the surrounding medium, size, density and shape of the particle, they are an excellent resource for monitoring the quality and reproducibility of the gold-nanoparticles monolayer [47–51]. For this section we have used the resonance location method to fabricate a high quality/highly reproducible monolayer of nearly spherical gold nanoparticles.

A previous work about the mechanisms of metal growing by sputtering [52] pointed out that there are two important considerations that must be made in order to grow a spherical monolayer?. First, the relationship between the initial nucleating centers and the particle density (Au-ρ); which cannot be changed for a determined substrate and second, the linear relationship between deposition time and particle average diameter (Au-Ø), which means that for longer deposition times, the bigger the Au-Ø.

However, nanoscale gold tends to agglomerate easily, for long deposition times these agglomerations results in nanoporous gold thin films rather than a homogeneous distribution of spherical particles. The location of the plasmonic resonance in a nanoporous gold thin film is difficult to reproduce because there are always slight changes in the location, even using identical deposition parameters. Those changes are attributed to an unpredictable location of the electric field surrounding the particles, because in nanoporous films there are not well defined particle shapes. Nevertheless, for spherical gold particles the reproducibility increases significantly, because the electrical field is located homogeneously around each particle forming the monolayer.

Therefore, to analyze and to correlate the particle characteristics of each growth we have defined the ratio $R_{Au} = Au\text{-}\rho/Au\text{-}\varnothing$. To avoid agglomeration we seek growths with the lowest Au-Ø. On the other hand, we needed to obtain the highest possible Au-ρ, because when the electrical fields around the particles work in a collective way, it is easier to identify the extinction plasmonic resonances of the gold monolayer. Therefore, it is possible to conclude that the higher the value of R_{Au} the better the specimen is for our purpose.

By using Sputtering technique, we carried out gold depositions on crystalline silicon wafers and quartz using short plasma times. We conducted ten growths with deposition times ranging from 1 to 10 seconds, and 1 s intervals between each deposition. Each specimen was named with the number of seconds used for its fabrication.

To determine the values of density and particle size diameter, a statistical study of the deposited AuNPs was performed. The particles were classified by size into 6 groups: Par-Ø≤1nm, 1nm<Par-Ø≤2nm, 2nm<Par-Ø≤3nm, 3nm<Par-Ø≤4nm, 4nm<Par-Ø≤5nm, 5nm<Par-

Ø≤6nm. About 50 HRTEM micrographs were obtained in different areas of each analyzed sample. The occurrence percentage of each particle group was reported in a histogram.

The described statistical analysis to obtain Au-ρ and Au-Ø was only done for depositions 4 and 5. This is because for depositions 1 and 2 it was almost impossible to detect AuNPs. In these samples we carried out observations at multiple different zones but the appearance of particles was rather sporadic. Compared to depositions 1 and 2, the sample 3 had a significant Au-ρ increase, however this sample was not subjected to analysis because at first glance its Au-ρ was estimated smaller than sample's 4.

After statistical analysis, sample 4 showed Au-ρ = 2.05E12 particles/cm^2, Au-Ø = 2.66 nm, and R_{Au} = 0.77. Meanwhile, in sample 5 was identified a good particle size homogeneity because of around 60% of the particles have sizes falling between 1 and 3 nanometers. The obtained results from sample 5 after the statistical analysis were: Au-ρ = 2.52E12 particles/cm^2, Au-Ø = 2.90 nm and R_{Au} = 0.86. The histogram of sample 5 can be found as supporting information (Supporting Figure 2).

A HRTEM micrograph showing the AuNPs distribution of sample 5 is shown in Figure 4. It is convenient to emphasize that particle distribution is uniform all over the sample and most of the particles have quasi-spherical shapes. Additionally, inset a) provides information concerning to the existing space between AuNPs; we measured in a random way some of those spaces, the resulting distances ranges from 0.8 to 1.5 nm. Evidently, this is purely qualitative information, because we did not make a formal statistical analysis of the separation distances. However, this is very powerful information because it allows us to understand what is happening with deposition times longer than 5 seconds. In the inset a), a small white box frames a pair of

particles that have collided during their growth. This phenomenon is not widespread in sample 5, but occasionally it is possible to notice that kind of fused particles.

As previously mentioned, the reproducibility was monitored by the location of the plasmonic resonances. The absorbance spectrum represented by the continuum line in the Figure 5 shows the plasmonic resonance location of the sample 5, which is located at 540±3nm. Several subsequent growths were made by using identical parameters to those used in sample 5, the location of the resonance and even the shape of the spectrum remain unaltered; the dotted line of Figure 5 displays an absorbance spectrum of any subsequent deposition using the sample 5 parameters.
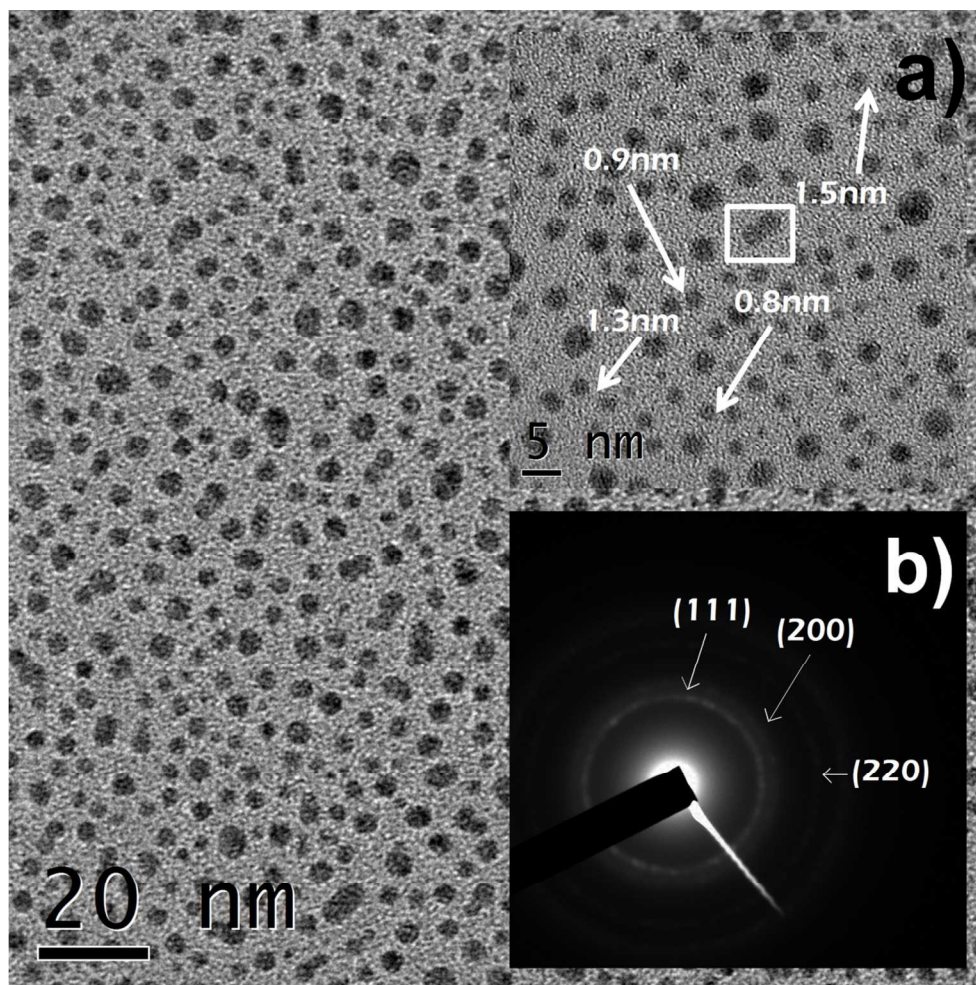
Figure 4. HRTEM micrograph obtained from sample 5, AuNPs with R_{Au} = 0.86 are deposited over silicon wafer. Uniform particle distribution and particle quasi-spherical shapes throughout the sample are observed. Inset a) shows the fused particle phenomenon when growth time is increased. Inset b) shows a characteristic gold diffraction pattern.
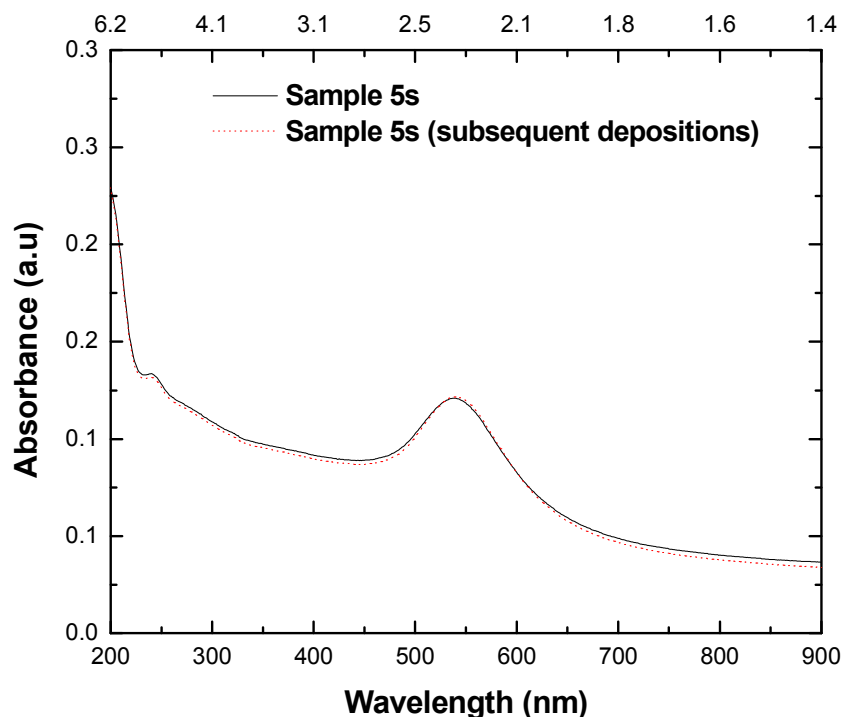
Figure 5. Absorbance spectrum of sample 5 (continuum line) and absorbance spectrum of any subsequent growth made using identical deposition parameters to those used in sample 5 (dotted line). The shape of the spectrum and the location of the resonance (540nm) remain unaltered, confirming a very high reproducibility.

For deposition 6, fused particles phenomenon is much more widespread than sample 5. About 30% of the nanoparticles in sample 6 have collided, forming a larger and irregular particle. The incidence of particle merging promotes an Au-ρ reduction and Au-Ø increment, which in turn results in a sharp drop of R_{Au} value. Low values of R_{Au} distort the resonance location and therefore its reproducibility; in samples 6 to 10 it is possible to estimate at first glance that R_{Au}

values are below 0.86. Therefore, beyond growth 5 any rise in deposition time will make R_{Au} to decrease until it reaches zero, which is the value for a nanoporous gold thin film. A Field Emission SEM micrograph from a 20 seconds deposition can be found in supporting information (Supporting Figure 3).

Engineering of the coupled silicon-gold structure

The aim of this fabrication methodology was to achieve a functional coupling between EMIS film and our selected AuNPs monolayer through the variation of the DIEL film thickness amongst them, in order to obtain an enhancement of photoluminescence from the coupled system. All tested structures were fabricated as follow: 1) deposition of a gold monolayer (AuNPs) over a silicon wafer, 2) deposition of a DIEL film over the AuNPs, 3) deposition of an EMIS film over the previously deposited DIEL layer. Deposition time of the DIEL layer was adjusted by steps of 30 seconds to get thicknesses of 5 nm, 10 nm, 15 nm, and so on. Meanwhile, deposition time was accurately adjusted to obtain EMIS films with thicknesses of 90 nm for all the fabricated structures.

In Figure 6 are showed the absorption spectra of some layered structures on quartz substrate: [i] absorption spectrum of DIEL layer (10 nm), [ii] absorption spectrum of gold nanoparticles surrounded by DIEL layer (10 nm), [iii] absorption spectrum of gold nanoparticles surrounded by EMIS film (90 nm). As it is expected, DIEL layer is transparent above 250 nm since stoichiometric silicon nitride has a band gap of ~5 eV. On the other hand, when the DIEL medium surrounds the AuNPs previously deposited on the substrate it is possible to observe the resonant peak of the local surface plasmon at ~538 nm (2.3 eV). Likewise, it can be noticed in the absorption spectrum of AuNPs/EMIS structure the presence of the metal nanoparticle resonance peak very close to that of the AuNPs/DIEL assembly in spite of different thickness of

the films. This high homogeneity of the silicon nitride phase of the DIEL and EMIS layers does

not distort in a high manner the resonance location of our gold monolayer, therefore the above

described multilayer structures will not change the initial properties of each layer used to

fabricate them.
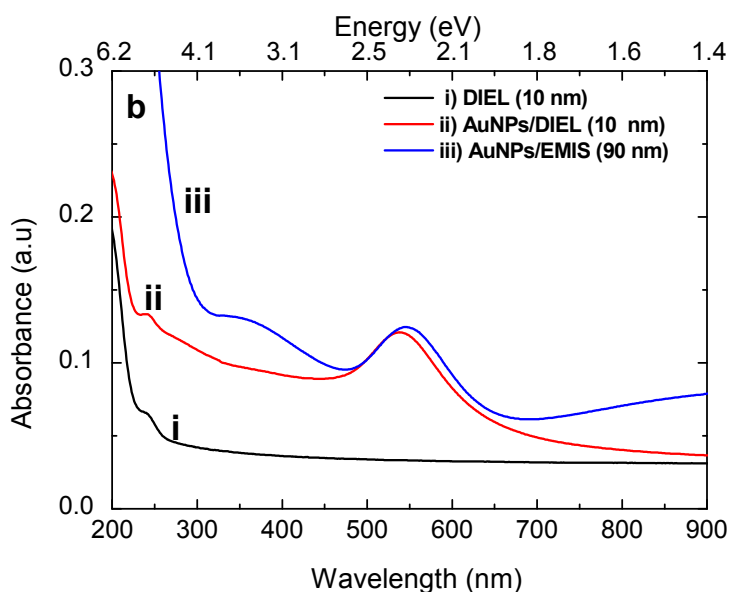
Figure 6. Absorption spectra of i) 10 nm of DIEL layer, ii) 10 nm of DIEL layer on AuNPs and iii) 90 nm of EMIS layer on AuNPs. All the layered structures were deposited on quartz. No considerable absorption peak-shift is observed in ii and iii despite different thickness of the films.

From Figure 7 can be observed four different configurations of the proposed structures using

DIEL layers of 0, 30, 60 and 90 seconds, which corresponded to thickness of 0, 5, 10 and 15 nm

respectively. For each configuration there was one sample as reference without AuNPs deposited

on the silicon substrate for comparative purposes, i.e., only steps 2) and 3) of the previously

described methodology were carried out for our control sample. PL spectra of the first

configuration devoid of a DIEL layer did not show change in the PL integrated intensity in spite

of the presence of Au nanoparticles in one of the structures (Figure 7a). In the second

configuration were grown 30 seconds of DIEL before the EMIS film deposition (Figure 7b). We

noted an enhancement ratio of 17% of the maximum PL peak and small red-shift (502 nm to 513

nm) from the coupled structure compared with the reference. The third configuration (Figure 7c)

using 60s of DIEL layer, showed an integrated PL enhancement of 105%, and an enhancement

of the maximum PL peak of 87% from the sample with AuNPs deposited. A smaller red-shift

(499 nm to 504 nm) compared with the second configuration is also noticed. Finally in Figure

7d, it is possible to observe a reduction of the PL intensity peak ratio up to 7% and practically no

peak-shift from the sample with AuNPs. This tendency of slight maximum PL peak enhancement

of the coupled samples with regard to their references is persistent for 120 and 150 seconds

corresponding to 20 and 25 nm of deposited DIEL layer, and can be observed in the scatter plot

of Figure 8.
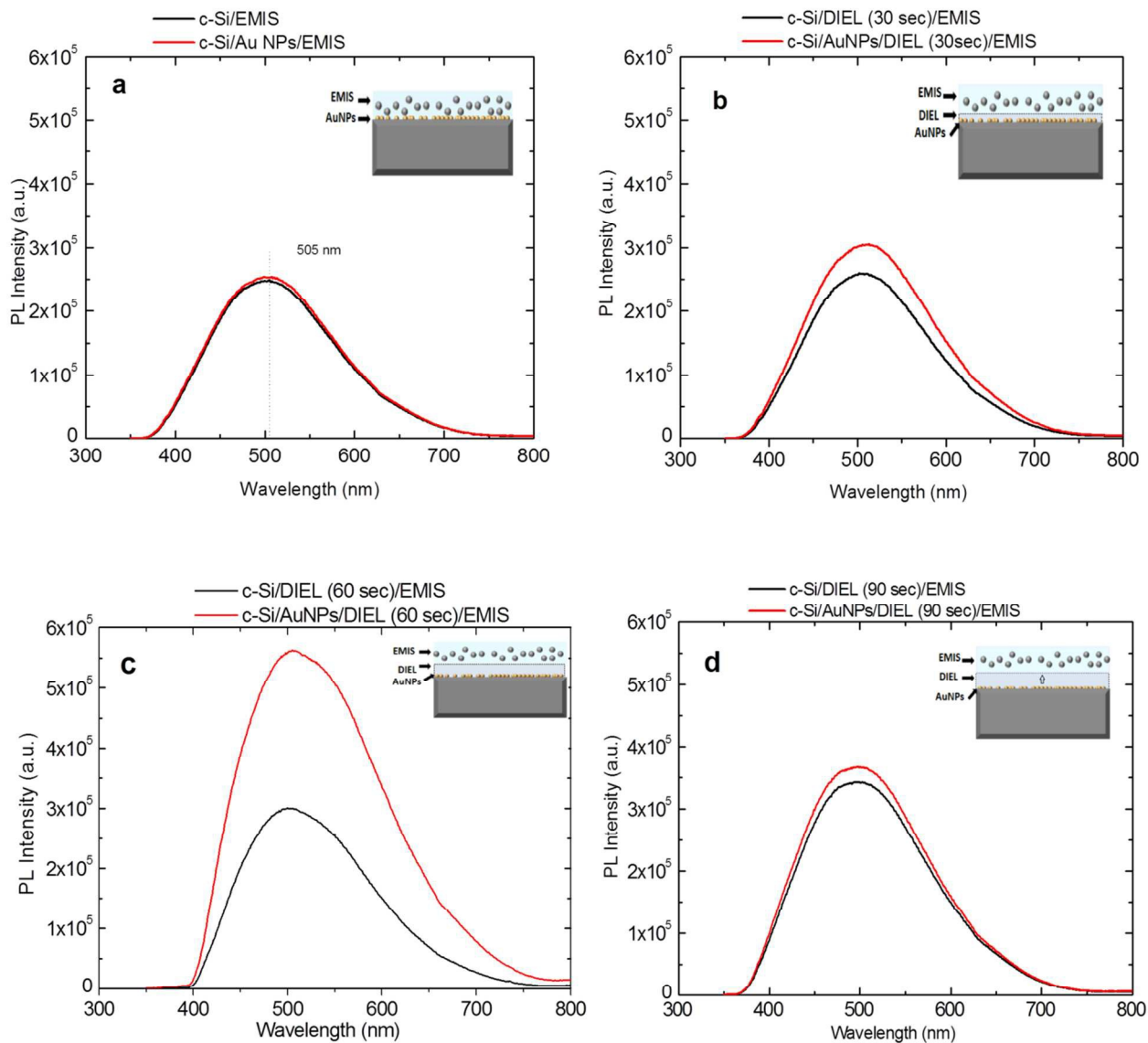
Figure 7. Four different configurations of the proposed structures using DIEL layers of 0, 30, 60 and 90 seconds, which corresponded to thickness of 0, 5, 10 and 15 nm respectively. Deposition time was adjusted for obtaining thickness of the EMIS films of 90 nm. For each configuration there was one sample used as reference without AuNPs deposited on the silicon substrate for comparative purposes. The major PL enhancement ratio was found for a thickness of the DIEL layer of 10 nm (schematic diagrams of the structures inside each graphic are not in scale).
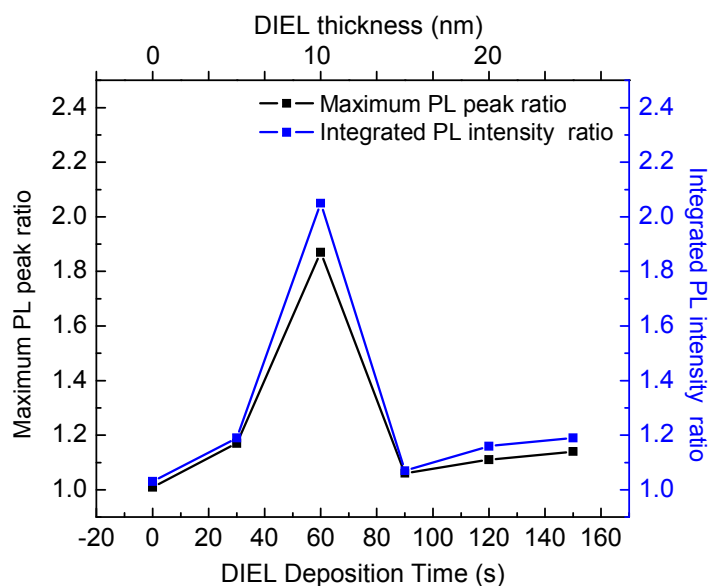
Figure 8. Scatter plot of the maximum PL peak ratio and integrated PL intensity ratio of the samples with 0, 30, 60, 90, 120 and 150 seconds of deposited DIEL layer.

As it was mentioned before, other researching groups have studied luminescence of structures metal-SiQDs as their separation distance get closer. They showed a Gaussian type PL enhancement ratio relative to their references[25–31]. This latter is not just an effect of bringing closer different material nanoparticles, but probably an effect of different particle density distribution through determined distances of the implanted zone. Consequently, it was difficult to define a maximum PL enhancement for a defined density concentration and separation distance among metal nanoparticles and silicon nanocrystals. In our experiment the homogeneous distribution achieved of the metallic monolayer and SiQDs radiative film let us to identify clearly that there is a well specific separation distance between the AuNPs/EMIS to attain maximum light enhancement in the system. It is worth mentioning that methodical reproduction of the experiment has confirmed 10nm DIEL thickness in our structures in order to achieve maximum light coupling.

21

We consider that there are two physical effects that could take place in the observed enhancement of these layered structures: a) coupling of the light from the emitter field, (i.e. EMIS layer) to the Localized Surface Plasmon Resonance (LSPR) of the AuNPs, and b) a change of the scattering mechanisms of the primary light (laser source of excitation) in the coupled structure.

The assumption of the enhancement due to the LSPR could be reasonable due to absorption-emission bandwidth of the SiQDs is wide enough to allow the coupling in a diffraction-limited way, as the one described by Kress et al [53]. This diffraction-limited coupling (DLC) has reported that a photon or exciton dipole coming from semiconductor nanocrystals with different sizes, (i.e. different energies) can couple to the local electric field surrounding the small gold nanoparticles. Then, the integrated structure will not only emit photons but also surface plasmon polaritons (SSPs) giving place to some little amount of the observed enhancement. This type of coupling also explains in some extent the slight redshifts observed from the coupled structures. However, it is not possible to attribute the whole enhancement to the LSRP coupling, because just one slice of SiQDs contained in the EMIS layer (which is 90 nm thick) is located at the correct distance to generate SPPs.

The other amount of the observed enhancement (and the bigger one) could be attributed to the seeded AuNPs beneath the EMIS layer in which SiQDs are contained. In its final configuration the multilayer structure will change the manner of scattering and interference of the primary light (He-Cd laser 325nm) and this should be the responsible of an increment in the photon density absorbed by SiQDs layer.

It is important to stand out that further theoretical and experimental studies are needed to determine and explain thoroughly the mechanisms responsible of the observed enhancements

and the contribution percentage of each one. However, from our work it is possible to affirm conclusively that an optimum separation distance between silicon quantum dots and gold nanoparticles is needed to achieve a PL enhancement.

Conclusions

In this paper we reported a new method for manufacturing a gold-silicon coupled structure which exhibited a PL integrated enhancement of 105%. Three stages were carried out for its manufacture: design of emitter field, design of gold nanoparticles and coupling between fields.

In first stage and due the quantum confinement effect, it was possible to us to tune the maximum PL peak from emitter field to 505nm, close enough to the resonance peak of gold nanoparticles, favoring the interaction between these two layers.

In gold nanoparticles design stage, we consider the convenience of a spherical particle because it concentrates electrical fields uniformly and therefore, just one peak of plasmonic resonance appears in a very reproducible manner. Meanwhile density and particle size played a major role regarding location of the resonance peak.

In third stage we found than a 10nm layer of silicon nitride generated the maximum possible enhancement. We believe that there may be two combined physical effects responsible of the enhancement: a) the LSPR diffraction-limited coupling and b) a change of the scattering mechanisms of the primary light.

Our results show the feasibility to manufacture silicon based structures with enhanced luminescence by using dry and low temperature techniques, such as those used in microelectronic industry.

Acknowledgements

Supporting Information

A HRTEM micrograph obtained from a DIEL film is showed in Figure 1. An histogram of sample 5, which are AuNPs deposited over silicon wafer is showed in Figure 2. A Field Emission SEM micrograph from a 20s deposition of AuNPs can be found in Figure 3.

References

1   D. Sarti and R. Einhaus, *Sol. Energy Mater. Sol. Cells*, 2002, **72**, 27–40.

2   A. Kingon, J. Maria and S. Streiffer, *Nature*, 2000, **406**, 1032–8.

3   M. Schulz, *Nature*, 1999, **399**, 729–730.

4   David J. Lockwood and Lorenzo Pavesi, *Silicon Photonics*, Springer Berlin Heidelberg, Berlin, Heidelberg, 2004, vol. 94.

5   D. Das and A. Samanta, *Phys. Chem. Chem. Phys.*, 2015, **17**, 5063–5071.

6   T.-W. Kim, C.-H. Cho, B.-H. Kim and S.-J. Park, *Appl. Phys. Lett.*, 2006, **88**, 123102.

RSC Advances Accepted Manuscript

7   T.-Y. Kim, N.-M. Park, K.-H. Kim, G. Y. Sung, Y.-W. Ok, T.-Y. Seong and C.-J. Choi, *Appl. Phys. Lett.*, 2004, **85**, 5355.

8   Y. C. Fang, Z. J. Zhang and M. Lu, *J. Lumin.*, 2007, **126**, 145–148.

9   A Irrera, P. Artoni, F. Iacona, E. F. Pecora, G. Franzò, M. Galli, B. Fazio, S. Boninelli and F. Priolo, *Nanotechnology*, 2012, **23**, 075204.

10   A. Rodriguez, J. Arenas and J. C. Alonso, *J. Lumin.*, 2012, **132**, 2385–2389.

11   W. Liao, X. Zeng, X. Wen, W. Zheng, Y. Wen and W. Yao, *J. Electron. Mater.*, 2015.

12   B. Sain and D. Das, *J. Lumin.*, 2015, **158**, 11–18.

13   B. M. Monroy, G. Santana, a Benami, a Ortiz, J. C. Alonso, J. Fandiño, F. Cruz-Gandarilla, J. Aguilar-Hernández, G. Contreras-Puente, a López-Suárez and a Oliver, *J. Nanosci. Nanotechnol.*, 2009, **9**, 2902–9.

14   R. Kumar Bommali, S. Preet Singh, S. Rai, P. Mishra, B. R. Sekhar, G. Vijaya Prakash and P. Srivastava, *J. Appl. Phys.*, 2012, **112**, 123518.

15   P. Nguyen, D. Kepaptsoglou, Q. Ramasse and a. Olsen, *Phys. Rev. B*, 2012, **85**, 1–8.

16   Y. Q. Wang, Y. G. Wang, L. Cao and Z. X. Cao, *Appl. Phys. Lett.*, 2003, **83**, 3474.

17   R. Walters, J. Kalkman, a. Polman, H. Atwater and M. de Dood, *Phys. Rev. B*, 2006, **73**, 2–5.

18   M. Estes and G. Moddel, *Phys. Rev. B*, 1996, **54**, 14633–14642.

19   F. Komarov, L. Vlasukova, I. Parkhomenko, O. Milchanin, a. Mudryi, a. Togambaeva and O. Korolik, *Thin Solid Films*, 2015, **579**, 110–115.

20   A. G. Nassiopoulos, S. Grigoropoulos and D. Papadimitriou, *Appl. Phys. Lett.*, 1996, **69**, 2267–2269.

21   L. Pavesi, L. Dal Negro, C. Mazzoleni, G. Franzò and F. Priolo, *Nature*, 2000, **408**, 440–4.

22   W. L. Ng, M. a Lourenço, R. M. Gwilliam, S. Ledain, G. Shao and K. P. Homewood, *Nature*, 2001, **410**, 192–194.

23   K. S. Cho, N.-M. Park, T.-Y. Kim, K.-H. Kim, G. Y. Sung and J. H. Shin, *Appl. Phys. Lett.*, 2005, **86**, 071909.

24   J. C. Alonso, F. a. Pulgarín, B. M. Monroy, a. Benami, M. Bizarro and a. Ortiz, *Thin Solid Films*, 2010, **518**, 3891–3893.

25   A. L. Tchebotareva, M. J. a De Dood, J. S. Biteen, H. a. Atwater and A. Polman, *J. Lumin.*, 2005, **114**, 137–144.

26   J. S. Biteen, D. Pacifici, N. S. Lewis and H. A. Atwater, *Nano Lett.*, 2005, **5**, 1768–73.

27   J. S. Biteen, N. S. Lewis, H. a. Atwater, H. Mertens and A. Polman, *Appl. Phys. Lett.*, 2006, **88**, 131109.

28   H. Mertens, J. S. Biteen, H. A. Atwater and A. Polman, *Nano Lett.*, 2006, **6**, 2622–2625.

29   J. S. Biteen, L. a. Sweatlock, H. Mertens, N. S. Lewis, a. Polman and H. a. Atwater, *J. Phys. Chem. C*, 2007, **111**, 13372–13377.

30   A. Benami, A. López-Suárez, L. Rodríguez-Fernández, A. Crespo-Sosa, J. C. Cheang-Wong, J. a. Reyes-Esqueda and A. Oliver, *AIP Adv.*, 2012, **2**, 012193.

31   A. Benami, Y. El Hassouani, A. Oliver and A. Lopez-Suarez, *Spectrosc. Lett.*, 2014, **47**, 411–414.

32   D. Li, F. Wang and D. Yang, *Nanoscale*, 2013, **5**, 3435–40.

33   F. Wang, D. Li, L. Jin, C. Ren, D. Yang and D. Que, *Opt. Lett.*, 2013, **38**, 2832–4.

34   F. Wang, D. Li, L. Jin, C. Ren, D. Yang and D. Que, *Opt. Express*, 2013, **21**, 1675–86.

35   F. Wang, M. Wang, D. Li and D. Yang, ***Opt. Mater. Express,*** 2012, **2**, 1437–1448.

36   E. Ozbay, *Science*, 2006, **311**, 189–193.

37   J. Fandiño, G. Santana, L. Rodríguez-Fernández, J. C. Cheang-Wong, a. Ortiz and J. C. Alonso, *J. Vac. Sci. Technol. A Vacuum, Surfaces, Film.*, 2005, **23**, 248.

38   A. Rodriguez-Gómez, A. García-Valenzuela, E. Haro-Poniatowski and J. C. Alonso-Huitrón, *J. Appl. Phys.*, 2013, **113**, 233102.

39   P. F. Trwoga, a. J. Kenyon and C. W. Pitt, *J. Appl. Phys.*, 1998, **83**, 3789.

40   A. Martínez, J. C. Alonso, L. E. Sansores and R. Salcedo, *J. Phys. Chem. C*, 2010, **114**, 12427–12431.

41   A. Rodríguez, J. Arenas, A. L. Pérez-Martínez and J. C. Alonso, *Mater. Lett.*, 2014, **125**, 44–47.

42　S. V. Deshpande, E. Gulari, S. W. Brown and S. C. Rand, *J. Appl. Phys.*, 1995, **77**, 6534–6541.

43　H. R. Philipp, *J. Electrochem. Soc.*, 1973, **120**, 295.

44　N.-M. Park, C.-J. Choi, T.-Y. Seong and S.-J. Park, *Phys. Rev. Lett.*, 2001, **86**, 1355–1357.

45　F. Giorgis, *Appl. Phys. Lett.*, 2000, **77**, 522–524.

46　M. Schnabel, C. Summonte, S. a. Dyakov, M. Canino, L. López-Conesa, P. Löper, S. Janz and P. R. Wilshaw, *J. Appl. Phys.*, 2015, **117**, 045307.

47　S. . Oldenburg, R. . Averitt, S. . Westcott and N. . Halas, *Chem. Phys. Lett.*, 1998, **288**, 243–247.

48　M. Hu, J. Chen, Z.-Y. Li, L. Au, G. V Hartland, X. Li, M. Marquez and Y. Xia, *Chem. Soc. Rev.*, 2006, **35**, 1084–1094.

49　E. J. R. Vesseur, R. De Waele, M. Kuttge and A. Polman, *Nano Lett.*, 2007, **7**, 2843–2846.

50　M. a Garcia, *J. Phys. D. Appl. Phys.*, 2012, **45**, 389501.

51　C. Noguez, *J. Phys. Chem. C*, 2007, **111**, 3806–3819.

52　M. Hirasawa, H. Shirakawa, H. Hamamura, Y. Egashira and H. Komiyama, *J. Appl. Phys.*, 1997, **82**, 1404–1407.

53　S. J. P. Kress, P. Richner, S. V Jayanti, P. Galliker, D. K. Kim, D. Poulikakos and D. J. Norris, *Nano Lett.*, 2014, **14**, 5827–5833.